Chapter 2

β1 Structure Prediction and Validation

2.1 Overview

Over several years, GPCR prediction methods in the Goddard lab have evolved to keep pace with the changing field of GPCR structure. Despite some success in the field with homology modeling, initial models based on existing crystal structures require some effort before they can be trusted to accurately reflect nuances of the desired system. (Chapter 4 details some of these efforts.) Over several years, Goddard *et al.* have developed,[70,78,79] applied,[53,80–88] and refined[71] techniques to determine the structure of GPCRs starting from the amino acid sequence and an initial template for arranging predicted TM regions in space.

The MembStruk method and its refinement in the GenSemble method begin by predicting the TM regions from the amino acid sequence, refining TM helices, then determining the rotations of the predicted helices in the membrane. TMPred[70,78] used a variation of the Eisenberg scale to determine the hydrophobicity of a position in an amino acid sequence and the hydrophobic moment of the helix. The

GenSemble method builds on the MembStruk method. PredicTM, like TMPred, uses an alignment of related sequences to determine the hydrophobicity along a sequence of interest, and uses moving window averages to reduce noise. It removes any gap penalty in the hydrophobic calculation by disregarding gaps in the target sequence or related sequences. It also uses the octanol scale,[89] a thermodynamic measurement, to determine hydrophobicity. This removes the need to adjust the hydrophobicity baseline in determining the starting and stopping point of helices. Both methods apply capping rules to extend predicted TM helices to charged or helix breaker residues. These hydrophobicites are used to calculate the hydrophobic center of the helices, which determines the vertical position of helices in the membrane.

Both methods build canonical helices and optimize them individually using short-term molecular dynamics in vacuum, with some changes in helix preparation and final structure choice, but the methods differ in the initial placement of these helices relative to each other. MembStruk aligns the optimized helices to the electron density map of the low-resolution frog rhodopsin structure.[17] It uses the hydrophobic center to position each helix along its axis, and hydrophobic moment to determine the helices' initial η rotation. GenSemble, developed as new GPCR crystal structures became more readily available, uses information either from fully optimized structure predictions (such as the prostaglandin receptor[84]) or from available X-ray structure data. Initial η values are less important because of refinements in the η rotation determination, so this initial rotation is determined

simply based on the conserved X.50 residue for the template and target structures. (TM3 uses 3.32, as the conserved 3.50 arginine is usually outside the predicted hydrophobic helix.)

MembStruk and GenSemble differ the most in their η rotation prediction procedures. While MembStruk rotates through 360° in 5° increments and optimizes each rotation with minimization only, GenSemble is built on the BiHelix and CombiHelix methods which optimize helix rotations with SCREAM.[90] This allows for rotation sampling in up to 30° increments. The BiHelix method isolates two helices at a time and samples every rotation of each helix (144 cases per pair), then combines the minimized pairwise energies to determine which TM bundles have the lowest energies for the system. The best bundles are built with CombiHelix and then optimized with SCREAM and short force-field minimization to determine the low-lying rotation combinations. The complete 360° sampling ensures that starting conformation is irrelevant to the method, and this has been verified with all available crystal structures.

Once predicted, a structure must be validated. Where ligand binding and mutation data are available, ligand binding site prediction is the method of choice. For some receptors, however, there is little ligand data. In addition, docking may introduce errors based on the binding site prediction method, and with methods still in development this technique may slow the validation of otherwise finalized structures. In the case of this β1 structure prediction, the timing necessitated swift prediction and validation, and there was a set of stabilizing mutation data avail-

able for validation.[91] Using SCREAM and minimization to mutate the predicted receptor structure to the mutants described for the impending crystal system, it is possible to validate the predicted β1 structure without the use of ligand binding predictions.

2.2 Methods

General Methods: All calculations were carried out using the DREIDING force field[92] with charges from CHARMM22.[93] Side chain placement was determined with SCREAM[90] Unless otherwise noted, all simulations were performed in the gas phase with a dielectric of 2.5.

2.2.1 Structure Prediction of the Turkey β1 Adrenergic Receptor

Prediction of transmembrane regions: We predicted the TM regions using PredicTM. First, we used NCBI BLAST[94] to obtain a set of 1,100 protein sequences homologous to the target receptor, including all adrenergic receptors from a variety of species. These sequences ranged from 7% to 56% sequence identity with turkey β1 (12 – 88% in TM regions). Next, we obtained the pairwise multiple-sequence alignment of these sequences using MAFFT,[95–97] modifying the result to compress gaps in the target sequence. We then used this alignment to determine the TM regions using a moving-window average hydrophobicity analysis based on the octanol scale.[89] The resulting hydrophobicity profile shows seven clear hydrophobic regions corresponding to seven TM helices (Figure 2.1). The final PredicTM he-

lices were determined by comparing the N- and C- termini of each helix to known "helix breaker" residues, typically glycine, proline, aspartic acid, glutamic acid, arginine, and lysine, and extending each TM region to include the nearest charged residue. The N-termini of TMs 1 and 3 were extended an additional three and four residues, respectively, upon comparison with the PredicTM-generated TM predictions of four related receptors: human β1 (P08588), turkey β4c (P43141), frog β1 (O42574), and human β2 (P07550). Table 2.1 shows the final TM predictions. Three sets of hydrophobic centers were calculated and carried forward to the next steps: "area" centers based on the area of the hydrophobicity peak, "rawmid" centers chosen as the geometric center of the helix, and crystal centers based on the 2RH1 β2 crystal structure.

Initial Helix Optimization (OptHelix) and Helix Bundle Assembly: After determining the sequence of each TM region, we optimized each TM individually using the OptHelix method.[71] Each TM is built individually as a polyalanine α-helix with Gly and Pro residues in locations corresponding to the target TM region. One extra residue was added to each end of each helix to stabilize the ends during this state. We minimized this helix with a conjugate gradient minimization, added Ser and Thr residues in appropriate locations using SCREAM, then performed short-term (2 ns) dynamics on each individual helix as described in Abrol, *et al.* The final helices were taken from the snapshot with an RMSD closest to that of the average structure during the last 1.5 ns of simulation. We removed the extra ala-

nine residues from the termini and arranged the finished helices in a seven-helix bundle using the orientations, distances, and tilt angles from the β2 human crystal structure (2RH1).[39] Although the alignment to the 1GZM bovine rhodopsin crystal template was evaluated, the resulting bundles had higher energies than those aligned to the β2 crystal, indicating it was a less favorable orientation. Only the results based on the β2 template are reported here in detail.

Helix Rotation Optimization (BiHelix/CombiHelix): The BiHelix/CombiHelix method determines the low-energy helix bundles for a system by considering combinations of helix rotations. This method is independent of the starting rotation. Twelve isolated pairs of helices are generated: 1–2, 1–7, 2–3, 2–4, 2–7, 3–4, 3–5, 3–6, 3–7, 4–5, 5–6, and 6–7. In each pair, each helix is rotated through 360° 30° increments, resulting in 144 combinations per pair. We optimize the sidechain orientations for each combination with SCREAM, then combine the pairwise energies using a mean field analysis to obtain the energy of each possible combination of rotations ($12^7 = 35$ million possibilities). We build the best 1,000 of these combinations, minimize for ten steps, then rank each of the top 1,000 bundles by energy.

For this work, the initial bundle was modified to allow polar interactions in the TM core to optimize fully. The ends of the TMs, those residues added at the end of the TM prediction process based on capping and consensus decisions, were mutated to alanine except for glycine and proline where appropriate. In the rest of the TM region, large, nonpolar residues (phenylalanine, isoleucine, leucine, va-

line, tryptophan, and tyrosine) were mutated to alanine. The BiHelix analysis was performed on this modified bundle. The best 1,000 structures were built with CombiHelix then mutated back to wild type residues. These structures were ranked by interhelical energies, determined by calculating the energy of each isolated helix, then subtracting it from the total calculated energy of the bundle.

2.2.2 Structure Mutation Calculations

We used SCREAM to replace sidechains in each mutant receptor and to simultaneously optimize residues within 5 Å of the mutated residue. This inclusion of surrounding residues is necessary to allow the receptor to adjust to the change in a reasonable way; for a mutation such as Val to Ala, surrounding residues may adjust to fill the gap, and for a mutation like Ala to Leu the opposite should be true. This 5 Å cavity was then minimized for ten steps to resolve steric conflicts, and single point energies were determined using the DREIDING force field. After this optimization, we converted the residues to neutral forms (to reduce possible bias due to long-range coulomb interactions) and determined both the total bundle energy and the interhelical interaction energy. A lower energy should correspond to a higher T_m, as both indicate a more stable structure.

2.3 Results and Discussion

Using PredicTM and the octanol scale, we obtained the seven TM regions based on the hydrophobicity of the β1 sequence and related sequences, shown in Fig-

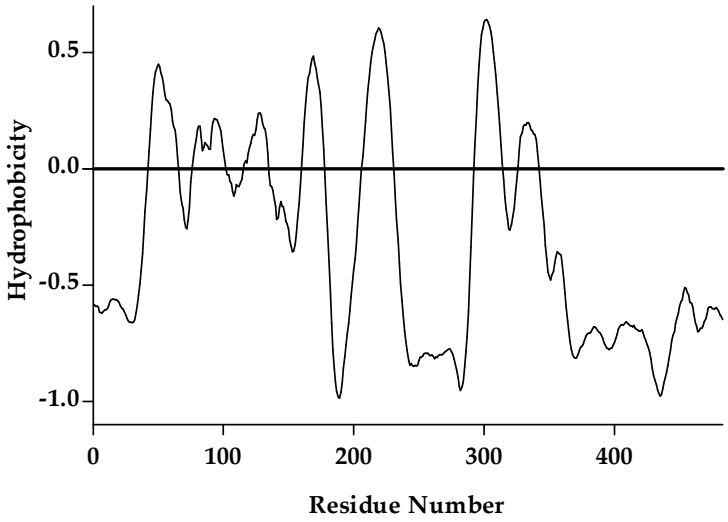

Figure 2.1: The hydrophobicity plot for $\beta 1$ turkey shows seven peaks representing to seven highly hydrophobic regions in the $\beta 1$ amino acid sequence. These regions correspond to the seven TM helices. These data were compared to similar plots for the human adrenergic receptors, and helices were lengthened to agree with the "consensus" predictions for the adrenergic family.

ure 2.1. These raw regions were lengthened based on comparison to the human adrenergic receptors; the differences between the raw predictions and the final predictions based on consensus are shown in Table 2.1. In general, the crystallographic helices are longer than the predicted helices, especially for TM3, since this prediction method relies solely on hydrophobicity rather than another indicator of helical character. In Chapter 4, this prediction method is supplemented with secondary structure predictions that consider helical character calculations as well as hydrophobicity. This consideration does produce helices closer in length to the crystallographic helices, but for the purposes of determining the TM core, the hydrophobicity and consensus analyses are sufficient to produce useful TM bundles.

After generating and optimizing the best 1,000 structures from the 35 million possibilities evaluated by BiHelix, several possibilities exist for choosing the best structure. Although ranking by minimized energy works consistently for BiHelix for crystallographic helices and 3D orientations, it is more difficult to encourage plausible combinations of rotations to appear within the top 0.05% of structures it is currently feasible to optimize. Selectively "alanizing" the input structure temporarily removes large nonpolar residues that might, as a result of the approximate template alignment, interfere with the formation of stabilizing polar contacts. It also eliminates the influence of polar or charged residues at the ends of the TM helices. In the native protein, these end residues can interact with the loops or charged lipid head groups. For the TM bundle calculations, however, these residues may distort the bundle rotation calculations and populate the top

Table 2.1: While the raw helices from PredicTM (β1 raw) are often truncated due to conserved polar and charged helices at the termini, comparison with other, related receptors provide plausible helices for structure prediction (β1 final). The 2VT4 β1 crystal sequence with α helical character is included for comparison, even though this data was not available at the time of these predictions. The raw midpoint hydrophobic centers are indicated in bold.

	β1 raw	AGMSLLMALV**V**LLIVAGNVLVIAAI
TM1	β1 final	QQWEAGMSLLMALV**V**LLIVAGNVLVIAAI
	β1 crystal	WEAGMSLLMALVVLLIVAGNVLVIAAIGST
	β1 raw	TNLFITSLACADL**V**MGLLVVPFGATLV
TM2	β1 final	TNLFITSLACADL**V**MGLLVVPFGATLVVR
	β1 crystal	TLTNLFITSLACADLVVGLLVVPFGATLVVRG
	β1 raw	CWTSLDVLCV**T**ASIETLCV
TM3	β1 final	SFLCECWTSLDVLCV**T**ASIETLCVIAID
	β1 crystal	GSFLCECWTSLDVLCVTASIETLCVIAIDRYLAI
	β1 raw	VIICTVWA**I**SALVSFLPI
TM4	β1 final	KVIICTVWA**I**SALVSFLPIMMH
	β1 crystal	TRARAKVIICTVWAISALVSFLPIMM
	β1 raw	YAIASSIISFY**I**PLLIMIFVYLRV
TM5	β1 final	RAYAIASSIISFY**I**PLLIMIFVYLRVYR
	β1 crystal	NRAYAIASSIISFYIPLLIMIFVALRAYREAKE
	β1 raw	GIIMGVFTL**C**WLPFFLVNIVNV
TM6	β1 final	KTLGIIMGVFTL**C**WLPFFLVNIVNV
	β1 crystal	REHKALKTLGIIMGVFTLCWLPFFLVNIVNVFN
	β1 raw	VFFNWLGY**A**NSAFNPII
TM7	β1 final	VFFNWLGY**A**NSAFNPIIYC
	β1 crystal	PDWLFVAFNWLGYANSAMNPIIYC

Table 2.2: When a selectively alanized structure is analyzed with BiHelix then the resulting bundles built and ranked by interhelical energies, many plausible structures appear in the top 100. The top 20 for turkey β1 aligned to the human β1 template using the raw midpoint centers are shown here.

H1	H2	H3	H4	H5	H6	H7	kcal/mol
30	240	60	210	30	30	270	-397.5
0	240	60	210	30	60	210	-383.9
270	30	60	210	60	0	330	-379.9
0	30	60	210	30	30	270	-379.8
30	240	60	210	30	30	120	-379.0
180	30	60	210	60	0	330	-378.5
0	30	60	120	60	0	330	-376.6
120	30	60	210	60	0	330	-374.7
30	330	60	210	30	30	270	-373.6
240	30	60	210	60	0	330	-372.5
0	300	90	120	60	0	60	-369.3
30	240	60	210	60	0	120	-367.9
0	30	60	210	30	30	330	-367.7
0	240	60	210	30	30	120	-366.9
0	30	60	210	30	30	0	-365.5
0	300	90	120	60	0	30	-365.4
90	30	60	210	60	0	330	-364.4
0	30	90	120	60	0	30	-363.8
0	30	60	210	60	0	330	-363.2
0	240	60	210	30	30	60	-362.9

1,000 structures with false positives. After these polar contacts are optimized by SCREAM and minimization, the larger nonpolar residues are restored and optimized. These full structures are then ranked by interhelical energy, which includes not only the polar interactions but any nonpolar interactions that may stabilize or destabilize the bundle. The best 20 of these structures are shown, ranked by interhelical energy, in Table 2.2.

The best structure by energy is based on the β2 2RH1 crystal structure template, using the raw midpoint hydrophobic centers (the geometric center of the hydrophobic helix prediction, before capping and TM extension to consensus se-

quences) to vertically orient the helices. This structure places most conserved residues in the appropriate positions for ligand binding and bundle stabilization. The TM1-TM2 salt bridge between Asn59$^{1.50}$ and Asp87$^{2.50}$ is closer to the protein-lipid interface than in related crystal structures, but the interaction itself (2.2 Å) is preserved. TMs 5, 6, and 7 are oriented such that Asp121$^{3.32}$, Ser212$^{5.43}$, Ser215$^{5.46}$, Trp303$^{6.48}$, Phe306$^{6.51}$, Asn310$^{6.55}$, Asn329$^{7.39}$, and Tyr333$^{7.43}$ are all accessible to the expected ligand binding pocket. This structure has an RMSD from the 2VT4 crystal structure of 3.7 Å and is close enough to a native conformation that it could be validated using the mutation data produced for the system. Figure 2.2 shows this structure with sidechains for binding site residues.

The experiments measured T_m for a series of mutations, defined as the temperature at which the protein begins to denature. After identifying point mutations that increased T_m for the mutant receptor, the group created and refined combinatorial sets of the best point mutations to eventually find the most stable mutant receptor that still preserved wild type binding and activation profiles. The final structure with the highest T_m contains six point mutations, but two of these (R68S and A282L) are expected to fall in the intracellular loops. As our methods focus primarily on the TM regions, any sets of mutations we consider must differ from one another without considering mutations sites in the loops. In order to ensure direct comparison between experimental and calculated energies, the mutations compared should also include the same loop residues.

With this in mind, we found three sets of mutations that fall within our pre-

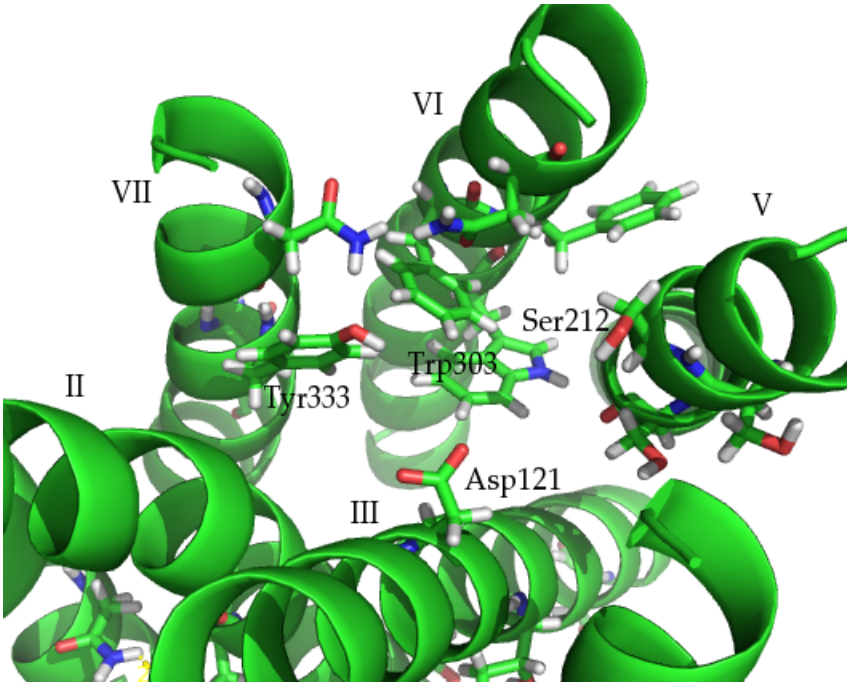

Figure 2.2: The top structure by interhelical energy shows most key residues for agonist binding oriented towards the binding pocket. Asp121$^{3.32}$ is particularly important for recognizing a protonated amine that is common to both agonists and antagonists. The conserved Trp303$^{6.48}$ and Phe306$^{6.51}$ are also oriented favorably. Ser215$^{5.46}$, part of the conserved adrenergic motif responsible for interaction with agonist catechol hydroxides, is also turned towards the binding pocket.

Table 2.3: Mutations probed include changes to TMs 2, 3, 5, and 7 in varying combinations. Set 1 includes m23, the combination of mutations eventually crystallized and reported as PDB 2VT1. T_m is listed relative to wild type.

	Label	T_m	2.53	2.61	3.40	5.58	5.61	7.32	7.37	7.44	7.48
Set 1	m6-11	7.4								A334L	
	m6-10	15.7				Y227A				A334L	
	m23	21.1	M90V			Y227A			F327A		F338M
Set 2	m4-6	3.3		G98A				D322A			
	m7-6	8.3	M90V		I129V						
	m7-5	13.5	M90V			Y227A					
	m7-7	13.5	M90V			Y227A					F338M
Set 3	m10-4	15.2	M90V				V230A			A334L	
	m10-8	15.6	M90V				V230A		F327A	A334L	
	m22	15.7	M90V			Y227A			F327A	A334L	
	m19	17.3	M90V			Y227A	V230A		F327A		F338M
	m18	17.9	M90V			Y227A			F327A		F338M

dicted TM bundle and affect T_m differently (summarized in Table 2.3). Set 1 includes mutations in TMs 2, 5, and 7: m6-11 with only A334$^{7.44}$L, m6-10 which adds Y227$^{5.58}$A, and m23 that adds M90$^{2.53}$V and replaces A334$^{7.44}$L with F327$^{7.37}$A and F338$^{7.48}$M. (This set includes the final combination of mutations that was characterized in the β1 crystal structure, m23.) Each of these experimental combinations also contains R68S (IC1) and A282L (IC3), residues not considered in the calculated energies. Set 2 begins with two pairs of different mutations: m4-6 with G98$^{2.61}$A and D332$^{7.32}$A, and m7-6 with M90$^{2.53}$V and I129$^{3.40}$V. Mutation combination m7-5 replaces I129$^{3.40}$V with Y227$^{5.58}$A, and m7-7 adds F338$^{7.48}$M to that combination. Set 3 contains the most combinations of mutations: five combinations of M90$^{2.53}$V, Y227$^{5.58}$A, V230$^{5.61}$A, F327$^{7.37}$A, A334$^{7.44}$L, and F338$^{7.48}$M. Each combination in set 3 includes R68S (IC1) that is not included in energy calculations.

The T_m and SCREAM energy data correlate significantly for sets 1 and 2, with

R^2 values ranging from 0.82 to 0.96. Set 2, shown in Figure 2.3, shows significant correlation for all four energy evaluations, while set 1 (Figure 2.4) correlates significantly for all evaluations except charged interhelical energies. For both sets, neutral evaluations show the strongest correlation and the closest fitting trendline. Neutral energies have been shown in the Goddard group to provide more reliable predictions, reduce noise in sampling, and increase resolution between structures that are expected to be closer in energy. Even in a dielectric, long-range coulomb interactions may play a role in force field energy calculations, a role that is not reflected in the reality of a protein solvated in water and lipid. Using a neutral residue scheme, the noise of long-range coulomb interactions is eliminated, resulting in more physical energies.

Despite the increased quality of energies calculated with a neutral residue scheme, the T_m values for set 3 are too close for a force field calculation to tell apart. The first three combinations shown in Table 2.3 span only 0.5, and the second two only 0.3, with the two groups only 1.6 apart, which is within experimental error for several of the cases. Even if precise, these differences correspond to an energy change of less than 0.01 kcal/mol which is not a reliable energy difference to probe with force field calculations. The combinations of mutations in sets 1 and 2 span 8 kcal/mol, which is a small change but reasonable to expect with the neutral residue paradigm. So while set 3 does not show agreement between the calculated mutation data and experimental T_m, the agreement with the wider energy ranges of sets 1 and 2 as well as the helix rotations placing known binding site residues in

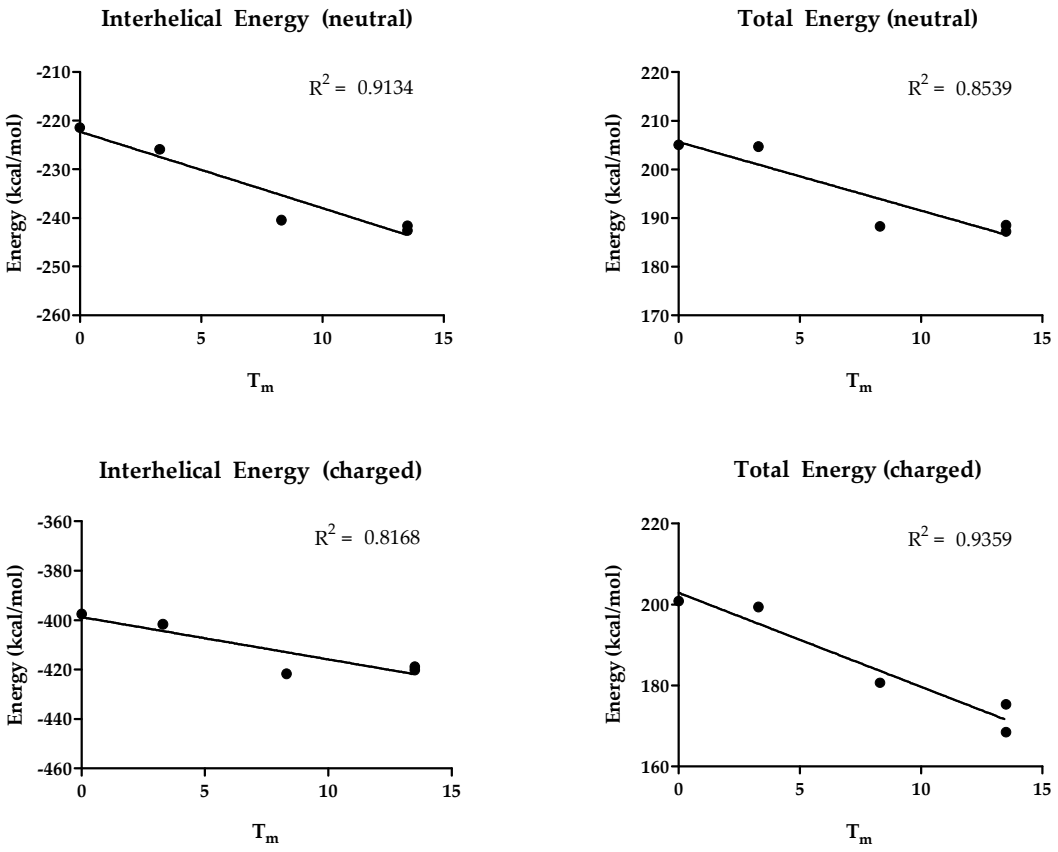

Figure 2.3: Set 2 shows the best overall correlation between calculation mutation energies and experimental T_m values, as all four energy evaluations correlate significantly with experiment. Note that the negative slope is expected, as an increase in T_m indicates the protein does not denature as easily and is therefore more stable, and a lower force field energy indicates a more stable structure.

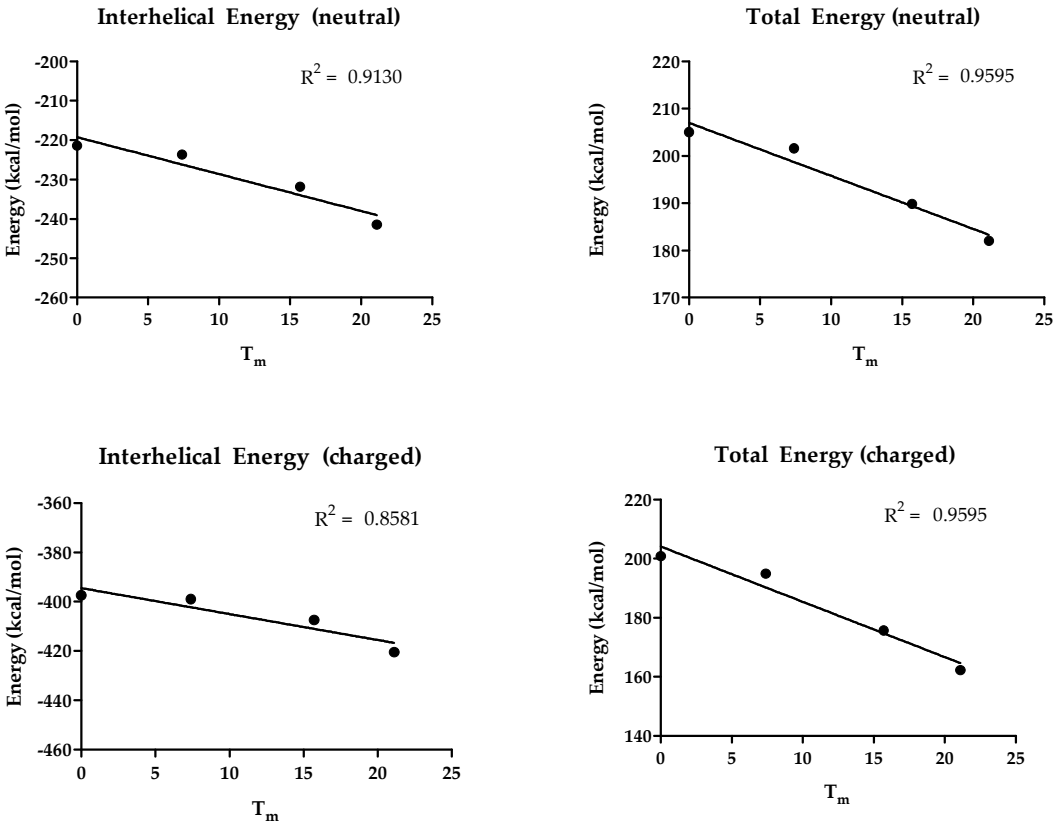

Figure 2.4: Set 1 shows significant correlation between calculated and experimental changes to turkey $\beta 1$ for both interhelical energy evaluations and the neutral total energy calculation. Using a neutral residue scheme allows for more accurate energy values, and should be considered a more reliable guide than the charged residue scheme.

expected locations near the agonist binding pocket give confidence that the predicted structure is indeed a valid conformation of the receptor.

2.4 Conclusion

Using the refined GenSemble method and stabilizing mutations reported in advance of the β1 crystal structure publication, a stable conformation for the turkey β1 adrenergic receptor was determined and validated. Although the resulting structure differed slightly from the eventual crystal data (CRMSD: 3.72 Å), the good agreement with the stabilizing mutations implies this structure is a valid alternate conformation for the system.

The validation study illustrates the utility of using neutral energies for comparison of structures. This approach has already enjoyed success in ligand docking studies (such as those discussed in Chapter 4 to validate homology models of the entire family of human adrenergic receptors) and is used here to confirm the agreement of this predicted structure with experimental data. It provides a sensible alternative to other methods of dampening spurious long-range coulomb interactions such as using a distance-dependent dielectric, and allows for confident calculation of smaller energy differences than a charged residue scheme.

Because the final predicted structure does have TMs 3, 5, 6, and 7 rotated such that important ligand binding residues are rotated inward towards the binding pocket, ligand docking studies may be performed. A docked β1-cyanopindolol complex with predicted intracellular and extracellular loops may also be equili-

brated in explicit water and lipid, similar to the procedures in Chapter 3. The structure may move towards the "native" structure observed in the crystal, or it may equilibrate to a different but similarly stable inactive conformation. This optimized structure may be a desirable starting point for further studies into GPCR activation, as it does not rely directly on a crystal structure for its initial conformation.